Citation
Liu, J. and Chen, W. and Hao, H. and Wang, Z. 2021. In-plane crushing behaviors of hexagonal honeycombs with different Poisson's ratio induced by topological diversity. Thin-Walled Structures. 159: ARTN 107223.
http://doi.org/10.1016/j.tws.2020.107223

In-plane crushing behaviors of hexagonal honeycombs with different initial Poisson's ratio (IPR) induced by topological diversity

Jiefu Liu[a,b,c], *Wensu Chen*[c], *Hong Hao*[c], *Zhonggang Wang*[a,b,d,e]*

a. School of Traffic & Transportation engineering, Central South University, Changsha, Hunan, China.

b. Key Laboratory of Traffic Safety on Track，Ministry of Education; Changsha, Hunan, China.

c. Centre for Infrastructural Monitoring and Protection, School of Civil and Mechanical Engineering, Curtin University, Australia.

d. Joint International Research Laboratory of Key Technology for Rail Traffic Safety, Changsha, Hunan, China.

e. National & Local Joint Engineering Research Center of Safety Technology for Rail Vehicle, Changsha, Hunan, China.

*wangzg@csu.edu.cn

Abstract In this study, the in-plane crushing behaviors of honeycombs with different initial Poisson's ratios (IPR) are investigated by means of analytical and numerical methods. The relationship between IPR value and cell geometry is established by using standard beam theory. The relationship between dynamic plateau stress and IPR value is also proposed. In addition, finite element model is built and calibrated first by using ABAQUS/Explicit. The specimens with different IPR values are then investigated under various crushing speed from 5 m/s to 150 m/s. A deformation-mode map is generated and the critical speed of changing deformation modes are determined. Based on the collapsed cell shape, a modified analytical model to predict the dynamic plateau stress is proposed. The specific energy absorption (SEA) of honeycombs with different IPR values is compared at different crushing speeds. The normalized plastic energy absorption is examined to study the strain rate effect on the energy absorption capacity.

Keywords: Initial Poisson's ratio (IPR), Honeycomb, In-plane crushing, Energy absorption.

1 Introduction

Sandwich structure with skins and various cores has been intensively investigated against impulsive loads [1-8]. Structure with hexagonal honeycomb core attracts wide attentions due to its superiority in mechanical properties and machinability [9-13]. Numerous studies have been carried out in terms of mechanical behavior and mechanism in the out-of-plane (which is perpendicular to the periodical direction) [14-18] and in-plane direction [19-21], respectively. The sound strength-to-weight ratio and energy absorption capacity of honeycomb subjected to crushing load have been demonstrated [21-25], which makes the honeycomb fit the requirements of the lightweight protective structures for structural and vehicle safety.

In the in-plane direction, the crushing behaviors are highly affected by the geometry of unit cell, attributing to the complex collapse mechanism that induced by either plastic hinge rotation or cell wall buckling [20, 23], and the influential factor such as the cell wall thickness has been investigated by many previous studies [21, 26]. With the development of manufacturing technique, a wide variety of hexagonal honeycombs with different cell configurations can be achieved in practice, e.g. re-entrant [1] and semi-re-entrant honeycomb [27] as shown in **Fig**. 1. Therefore, the studies on the influence of diverse cell configurations on crushing behaviors were carried out. Hu et al. [28] discussed the in-plane crushing response of conventional hexagonal honeycomb with varied cell wall inclined angles and it was found that the inclined angle significantly affects the deformation mode and crushing strength. Amin et al. [22] studied the influence of functionally graded design on the crushing response of honeycomb, an enhancement of energy absorption has been found with the strong to soft cell arrangement from the impact end to the support end. Liu et al. carried out the comparative study on the re-entrant and conventional honeycomb in terms of crushing behavior [1] and close-in blast resistance [29]. It was found that re-entrant cell has better performance due to the contraction effect subjected to the loading. More studies about the influence of cell configuration on the in-plane mechanical behaviors can be referred to the studies [30, 31].

Most of the previous works focused on the influence of individual geometric parameter (such as cell angle and length) on the mechanical behavior. However, there was very limited study on the influence induced by the cell topology. A topological evolution map of hexagon honeycomb cells is presented in **Fig**. 1 by adjusting the cell wall inclined angle and cell wall length. Different from the previous investigations, this study aims at investigating the influence of topological diversity on the in-plane crushing behavior. The topologies include re-entrant, semi-re-entrant and convex honeycomb structures, representing negative, zero, and positive initial Poisson’s ratio, respectively. The initial Poisson’s ratio (IPR) is expressed with respect to cell topology. The relationship between dynamic plateau stress and IPR of honeycomb matrix is established. In addition, the influences of IPR on the dynamic plateau stress, densified strain and specific energy absorption (SEA) are discussed.

2 Analytical study

2.1 Relationship between IPR and topological diversity

In this study, the initial Poisson's ratio (IPR) of unit cell is changed to represent various cell topologies. **Fig**. 1 gives the topological evolution map of honeycombs with different IPR values. The schematic diagram of representative cell model used to calculate the IPR is shown in **Fig**. 2. In this study, the crushing load is only applied in the in-plane vertical direction (i.e. y direction) and only the IPR v_{xy} is of interest herein. The analytical model to calculate the IPR of honeycombs is based on the standard beam theory and assumes bending deformation only [9, 19]. For the hexagonal honeycombs, because the horizontal cell wall is perpendicular to the loading direction, only the mechanical analysis on the inclined cell wall needs to be conducted (red highlighted in **Fig**. 2). When subjected to a vertical force *F*, the deflection δ of individual inclined cell wall is expressed as:

$$\delta = \frac{Fl^3}{12EI} sin\,\theta \tag{1}$$

Projecting the deflection in the horizontal (x direction) and vertical direction (y direction), respectively [9]:

$$\delta_x = \frac{Fl^3}{12EI} sin\,\theta\, cos\,\theta \tag{2}$$

$$\delta_y = \frac{Fl^3}{12EI} (sin\,\theta)^2 \tag{3}$$

According to **Fig**. 2, the deformation of re-entrant and convex cell in x direction is equal in magnitude but has opposite sign, and that of semi-re-entrant cell is zero. The deformation in x direction for different unit cells can be therefore defined as:

$$\delta_1 = -2\delta_x \quad \text{for re-entrant} \tag{4a}$$

$$\delta_1 = 0 \quad \text{for semi-re-entrant} \tag{4b}$$

$$\delta_1 = 2\delta_x \quad \text{for convex} \tag{4c}$$

Correspondingly, the effective strain in x direction ε_x can be defined as the ratio of the deformation δ_1 to the dimension of cell in x direction:

$$\varepsilon_x = \frac{\delta_1}{L_x} = \frac{Fl^3 \, sin\,\theta\, cos\,\theta}{6EI(h+l\,sin\,\theta)} \quad \text{for re-entrant } \theta < 0 \tag{5a}$$

$$\varepsilon_x = \frac{Fl^3 \, sin\,\theta\, cos\,\theta}{6EI(h+l\,sin\,\theta)} \quad \text{for semi-re-entrant } \theta = 0 \tag{5b}$$

$$\varepsilon_x = \frac{Fl^3 \, sin\,\theta\, cos\,\theta}{6EI(h+l\,sin\,\theta)} \quad \text{for convex } \theta > 0 \tag{5c}$$

The deformation of different cells in y direction is the same, the deformation and effective strain in y direction can be therefore defined as:

$$\delta_2 = -2\delta_y \tag{6}$$

$$\varepsilon_y = \frac{\delta_2}{L_y} = -\frac{Fl^2\,(\sin\theta)^2}{12EI\cos\theta} \tag{7}$$

The initial Poisson's ratio is therefore defined as the ratio of effective strain in x direction to that in y direction:

$$v = -\frac{\varepsilon_x}{\varepsilon_y} = \frac{(\cos\theta)^2}{\sin\theta\left(\frac{h}{l}+\sin\theta\right)} \quad \text{for re-entrant } \theta < 0 \tag{8a}$$

$$v = \frac{(\cos\theta)^2}{\sin\theta\left(\frac{h}{l}+\sin\theta\right)} \quad \text{for semi-re-entrant } \theta = 0 \tag{8b}$$

$$v = \frac{(\cos\theta)^2}{\sin\theta\left(\frac{h}{l}+\sin\theta\right)} \quad \text{for convex } \theta > 0 \tag{8c}$$

Fig. 3 gives the orthogonal analysis results regarding the influence of geometry (θ and h/l) on the IPR values. The cell wall ratio (h/l) changes from 1 to 5 and the angle (θ) varies between -60^0 and 60^0. In **Fig**. 3, the extremums of negative and positive IPR are marked as A and E. The specific values of IPR ± 1 (B and D) are also noted. It is found that the lower θ and h/l leads to a slender unit cell, e.g. the cells A and E in **Fig**. 3, which is prone to produce transverse displacements and therefore yields the higher absolute value of IPR. The red plane represents the distribution of IPR of semi-re-entrant cells and it is found that the zero IPR marked as C is not affected by the geometry.

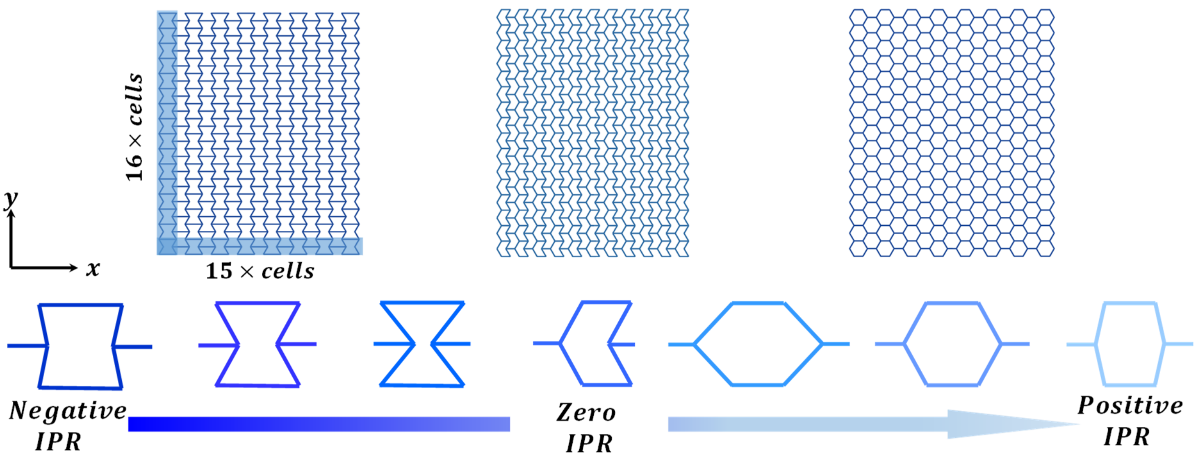

Fig. 1. Topological evolution map of hexagonal honeycombs with different initial Poisson's ratios (IPR).

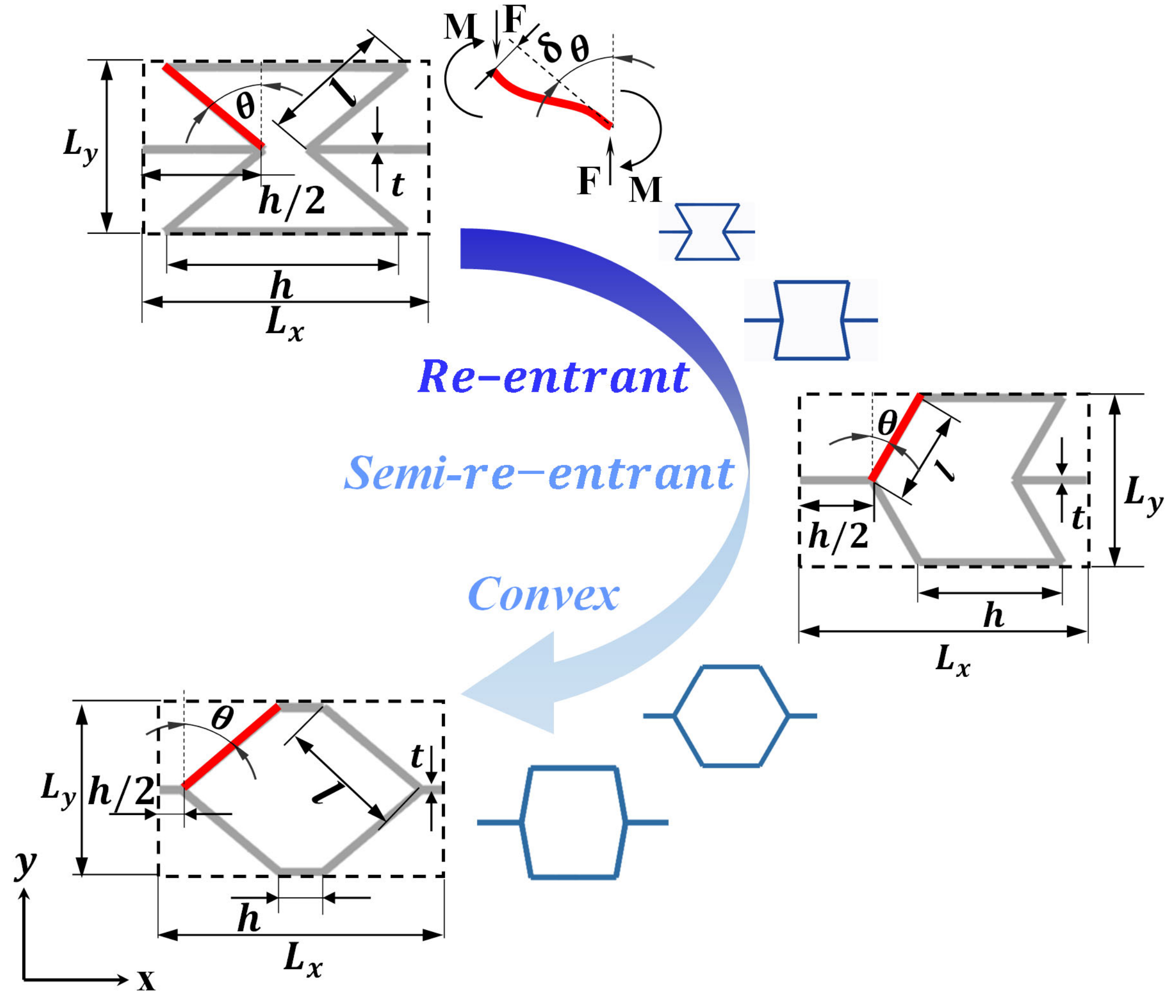

Fig. 2. Schematic diagram of representative cells.

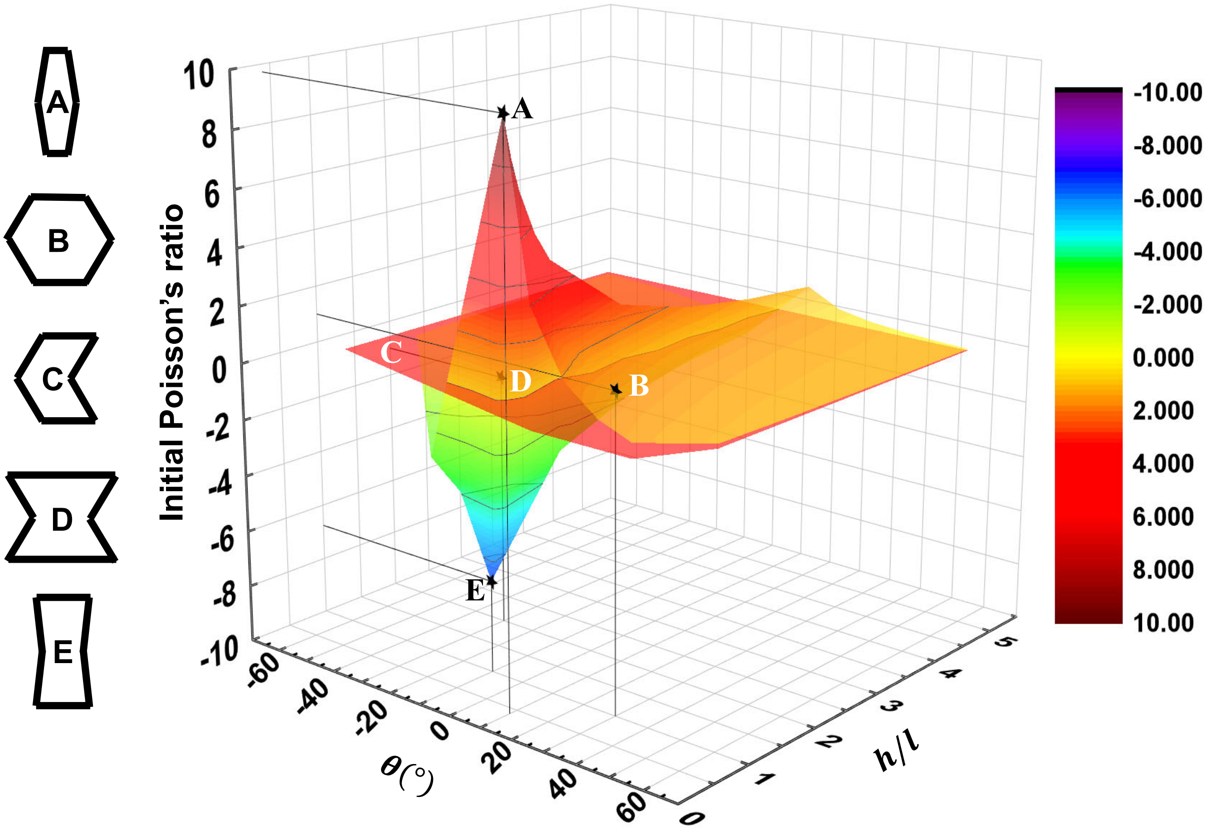

Fig. 3. The relationship between IPR values and the geometry (θ and h/l).

2.2 Plateau stress for high speed crushing

Plateau stress is one of the most important mechanical properties for the cellular materials as it significantly affects the energy absorption capacity [9, 21]. To theoretically analyze the dynamic plateau stress of honeycombs with different IPR, one dimensional shock model for cellular materials proposed in Ref. [32] is adopted herein. According to the model, the dynamic plateau stress σ_d can be simplified as a function of σ_0, crushing speed V, relative density ρ^* and densified strain ε_d [32]:

$$\sigma_d = \sigma_0 + \frac{\rho^*}{\varepsilon_d} V^2 \tag{9}$$

where σ_0 is the static collapse stress of honeycomb and it is correlated with the geometry of unit cell and the yield stress σ_y of the base material. By balancing the maximum bending moment of the inclined cell wall (highlighted in **Fig**. 2) and the fully plastic bending moment of a standard beam, σ_0 can be written as:

$$\sigma_0 = \frac{\sigma_y t^2}{2l(h + l\sin\theta)|\sin\theta|} \quad \text{for re-entrant } \theta < 0 \tag{10a}$$

$$\sigma_0 = \frac{\sigma_y t^2}{2l|\sin\theta|h} \quad \text{for semi-re-entrant} \tag{10b}$$

$$\sigma_0 = \frac{\sigma_y t^2}{2l(h + l\sin\theta)|\sin\theta|} \quad \text{for convex } \theta > 0 \tag{10c}$$

Some previous works [23, 33] proposed a collapse period analysis based on a representative deformation element (RDE) to calculate the dynamic plateau stress. Such method is adopted herein to derive the dynamic plateau stress. Through observing the deformation pattern of honeycombs under a relative high crush speed (70 m/s in **Fig**. 4 (a)), a localized 'I' shape (highlighted region) collapse band occurs in the deformed area [21, 33] and the rest part almost remain undeformed. Due to the periodicity of the collapse process, the dash red rectangle area should experience similar collapse process as the solid red rectangle area. The RDE can therefore be extracted from the layer that just in front of the deformed area with two longitudinally arranged cells, as shown in **Fig**. 4 (a).

To derive the dynamic plateau stress, some basic assumptions should be given. As shown in **Fig**. 4 (b), the cells above the RDE were fully crushed and those below the RDE remain undeformed which is named as the localized deformation assumption. Herein, the analytical model can only be applied to those situations which satisfying the localized deformation assumption and the detail discussion will be given in section 4.2. The stress applied on the RDE is therefore assumed as dynamic plateau stress σ_1 and the reaction stress is assumed as static plateau stress σ_0. The contraction and expansion of the RDE induced by the IPR effect was found less than 5% in previous study [28] and it is therefore ignored here, the dimension of RDE in x direction is assumed as constant throughout the collapse period (e.g. $L_0 = L_1$).

As shown in **Fig**. 4 (b), different colors of the struts represent different motion states (i.e. different momentums). The blue, red and green colors represent the struts with non-zero momentum, the black color represents the struts in still. The momentum of the RDE at $T = T_0$ can be therefore given as:

$$P_{t0} = P_{12} + P_{23} + P_{34} + P_{45} + P_{56} + P_{27} + P_{58} \tag{11}$$

The momentum of the RDE at $T = t_1$ can be given as:

$$\begin{aligned} P_{t1} = {} & P_{1'2'} + P_{2'3'} + P_{3'4'} + P_{4'5'} + P_{5'6'} + P_{2'7'} + P_{5'8'} + P_{7'8'} + P_{7'10'} + P_{8'11'} \\ & + P_{9'10'} + P_{10'13'} + P_{11'14'} + P_{11'12'} \end{aligned} \tag{12}$$

Due to the periodicity of the collapse process, the struts in the same color have the same motion state as shown in **Fig**. 4 (b):

$$\begin{aligned} P_{12} = P_{9'10'}, P_{23} = P_{7'10'}, P_{34} = P_{3'4'}, P_{45} = P_{8'11'}, P_{56} = P_{11'12'}, P_{27} \\ = P_{10'13'}, P_{58} = P_{11'14'} \end{aligned} \tag{13}$$

According to the theorem of linear momentum:

$$bL_0 \int_{T_0}^{T_1} (\sigma_1 - \sigma_0) dT = P_{T1} - P_{T0} \tag{14}$$

By incorporating Eqs. (11), (12) and (13), Eq. (14) can be rewritten as:

$$bL_0 \int_{T_0}^{T_1} (\sigma_1 - \sigma_0) d_t = P_{1'2'} + P_{2'3'} + P_{4'5'} + P_{5'6'} + P_{2'7'} + P_{5'8'} + P_{7'8'} \tag{15}$$

where b is the out-of-plane thickness of the honeycomb matrix. The momentum in Eq. (15) can be given as:

$$\begin{gathered} P_{1'2'} = P_{5'6'} = \frac{\rho_0 thbV}{2} \\ P_{7'8'} = \rho_0 thbV \\ P_{2'3'} = P_{4'5'} = P_{2'7'} = P_{5'8'} = \rho_0 tlbV \end{gathered} \tag{16}$$

where ρ_0 refers to the base material density and other parameters are given in **Fig**. 2. Assuming the dynamic plateau stress keeps constant in the short collapse period and the time interval is given as $T_1 - T_0 = (H_0 - H_1)/V$, Eq. (15) can be simplified as:

$$bL_0(\sigma_d - \sigma_0)(H_0 - H_1)/V = 2\rho_0 tbV(h + 2l) \tag{17}$$

The dynamic plateau stress σ_d is derived as:

$$\sigma_d = \frac{2\rho_0 tV^2(2l + h)}{(H_0 - H_1)L_0} + \sigma_0 \tag{18}$$

H_0 at $T = T_0$ can be considered as the height of undeformed RDE:

$$H_0 = 4l \cos\theta \tag{19}$$

H_1 at $T = T_1$ consists of the height of one uncollapsed and one fully crushed cell:

$$H_1 = 2l \cos\theta + \alpha t \tag{20}$$

Noting that αt is the height of fully crushed cell and it varies for honeycombs with different topologies. For the re-entrant and semi-re-entrant honeycombs, α is 4 as given from **Fig**. 4 (b). For the convex honeycombs, α is 2.67 as given in the previous work [23]. L_0 refers to the dimension of cell in x direction and it has the same expression for the re-entrant and convex honeycombs:

$$L_0 = 2(h + l \sin\theta) \tag{21}$$

For the semi-re-entrant honeycombs:

$$L_0 = 2h \tag{22}$$

Substitute Eq. (19) ~ (22) and Eq. (10) into Eq. (18):

(23a)

$$\sigma_d = \frac{\rho_0 tV^2(2l+h)}{(h+l\sin\theta)(2l\cos\theta-\alpha t)} + \frac{\sigma_y t^2}{2l(h+l\sin\theta)|\sin\theta|} \quad \text{for re-entrant } \theta < 0$$

(23b)

$$\sigma_d = \frac{\rho_0 tV^2(2l+h)}{h(2l\cos\theta-\alpha t)} + \frac{\sigma_y t^2}{2l|\sin\theta|h} \quad \text{for semi-re-entrant}$$

(23c)

$$\sigma_d = \frac{\rho_0 t V^2 (2l+h)}{(h+l\sin\theta)(2l\cos\theta-\alpha t)} + \frac{\sigma_y t^2}{2l(h+l\sin\theta)|\sin\theta|} \quad \text{for convex } \theta > 0$$

When $\theta = 30^0$ and $h = l$, the same results as that in Ref. [23] can be achieved, i.e., the results in [20] is a special case of Eq. (23). In Eq. (23), the first term is related to the crushing speed and the second one is related to the material properties. Therefore, Eq. (23) can be simplified with a static coefficient A and a dynamic coefficient B as below:

$$\sigma_d = A\sigma_y + \rho_0 V^2 B \tag{24}$$

$A\sigma_y$ represents the static plateau stress σ_0 in Eq. (9) and $\rho_0 V^2 B$ represents the inertia effect $(\rho^*/\varepsilon_d)V^2$ in Eq. (9), where A and B only relate to the cell geometry which can be expressed as:

$$A = \frac{t^2}{2l(h+l\sin\theta)\,|\sin\theta|} \quad \text{for re-entrant } \theta < 0 \tag{25a}$$

$$A = \frac{t^2}{2l\,|\sin\theta| h} \quad \text{for semi-re-entrant} \tag{25b}$$

$$A = \frac{t^2}{2l(h+l\sin\theta)\,|\sin\theta|} \quad \text{for convex } \theta > 0 \tag{25c}$$

$$B = \frac{(2l+h)t}{2(h+l\sin\theta)(l\cos\theta-\alpha t)} \quad \text{for re-entrant } \theta < 0 \tag{26a}$$

$$B = \frac{(2l+h)t}{h(2l\cos\theta-\alpha t)} \quad \text{for semi-re-entrant} \tag{26b}$$

$$B = \frac{(2l+h)t}{2(h+l\sin\theta)(l\cos\theta-\alpha t)} \quad \text{for re-entrant } \theta > 0 \tag{26c}$$

Fig. 5 gives the coefficients A and B with respect to different IPR values, respectively, where a specific cell wall thickness t is used. The red line shows the relationship between static coefficient A and different IPR values. Since the honeycombs with the IPR of the same magnitude but opposite sign (e.g. ± 1) have the same geometry (θ and l), the coefficient A is symmetrical to the zero IPR. From Eq. (26), coefficient A is inversely proportional to the θ and l. Since larger absolute value of IPR induces smaller θ and l, the coefficient A therefore increases with the rising absolute value of IPR. The blue curve represents the relationship between coefficient B and IPR. The magnitude of coefficient B is found much higher than A, which indicates that inertia effect is a dominant factor for the dynamic plateau stress. Coefficients A and B of honeycombs with zero IPR are also given in **Fig**. 5. It is found that the zero IPR has the same coefficient A as IPR $= \pm 1$ because of the same geometry (θ and l). The coefficient B for the case of zero IPR ranges between those of negative and positive IPR.

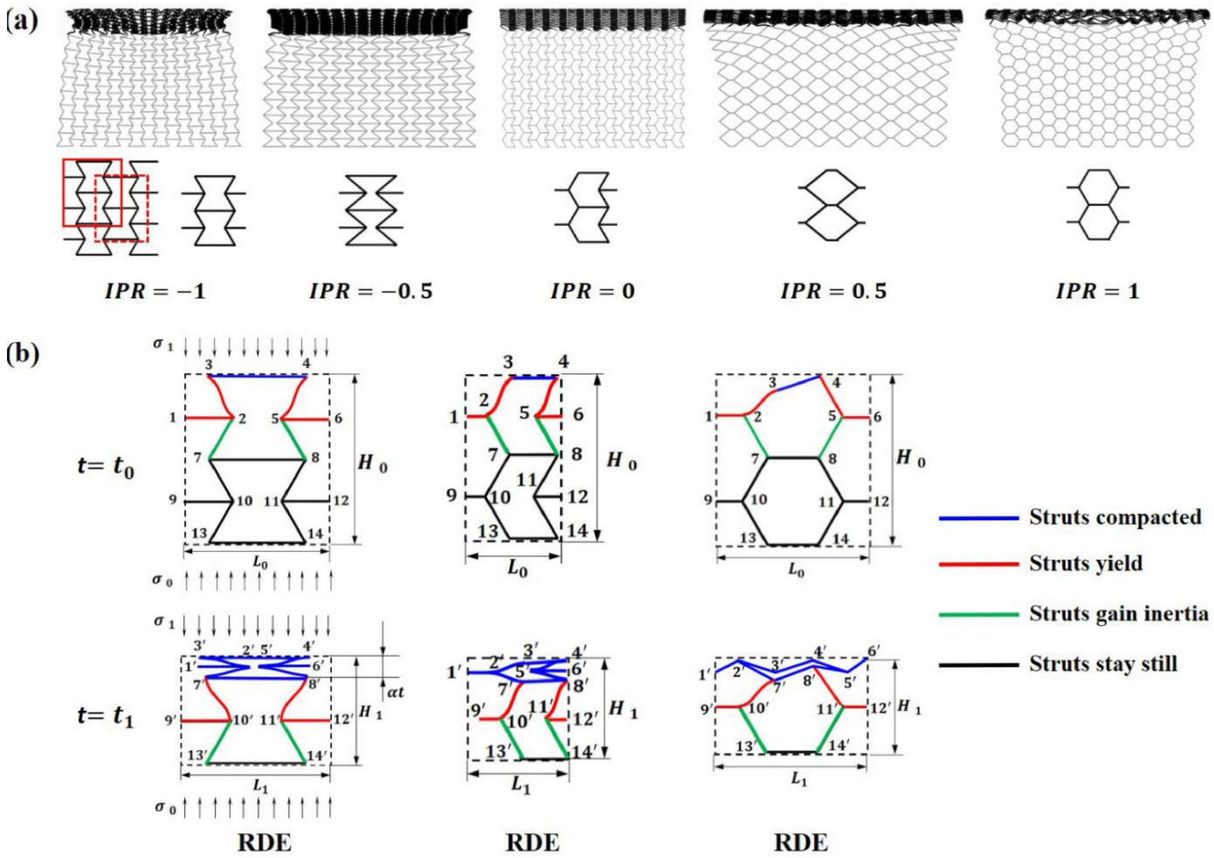

Fig. 4. (a) Collapse modes of different honeycombs with 'I' shape collapse band [21, 33] (highlighted region) and the representative deformation elements (RDEs) which are framed by the solid and dotted red lines; (b) Representative deformation elements (RDEs) at the initial state ($t = t_0$) and the final state of collapse period ($t = t_1$).

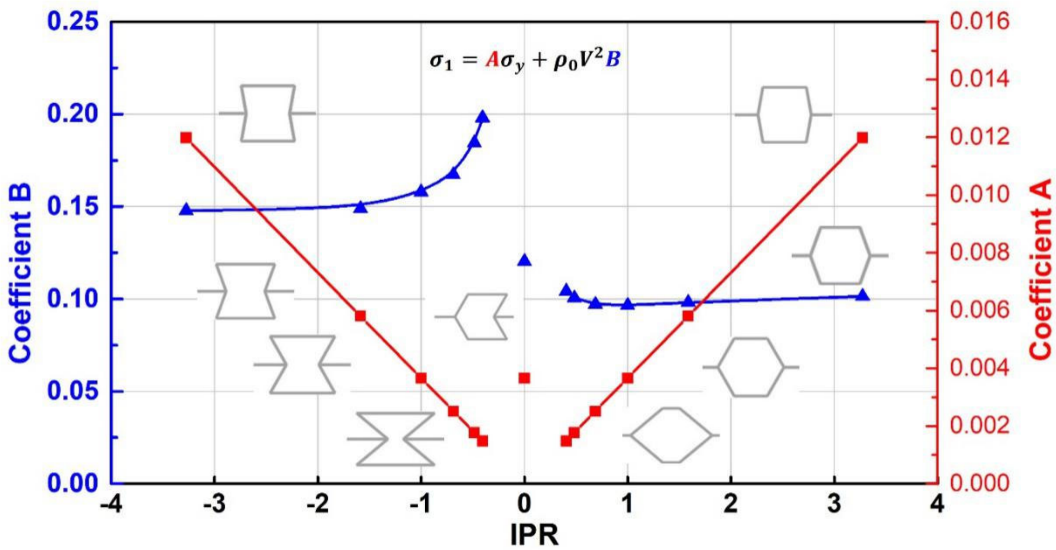

Fig. 5. Relationship of coefficient A and B with respect to various IPR values (to avoid the influence of cell wall thickness, presumably a specific thickness 0.2 mm is used).

3 Numerical model calibration

Numerical simulations are conducted by using finite element code ABAQUS/Explicit. The numerical model is similar to that in [1, 21] and the specific model setup is elaborated below. The honeycomb structure consists of 15×16 cells, the cell wall thickness and the out-of-plane dimension are kept as 0.2 mm and 1 mm, respectively, as shown in **Fig**. 1. The honeycomb structure is placed on a clamped rigid plate and crushed by the top rigid plate. In this study, the characteristics of the crushing behavior are identified with the crushing speed varied from 5 to 150 m/s (i.e. strain rate range: $66.6 - 2000\ \mathrm{s}^{-1}$), which is covered in the previous studies [1, 21].

The honeycomb structures are modelled by shell element with reduced integration (S4R). The hourglass control algorithm is used to avoid hourglass energy during the analysis. The general contact algorithm in ABAQUS with the properties of tangential behavior (friction coefficient 0.2) and hard contact is implemented to simulate the contact behaviors [33]. Mesh convergence studies are conducted and the mesh size of 0.5 mm is determined. Periodic boundary condition is applied along the out-of-plane direction of the model and only in-plane motion is allowed. In the FE models, the aluminum foil material is modeled as elastic, perfectly plastic material without strain rate effect. The aluminum material has Young's modulus of 69 GPa, Poisson's ratio of 0.33 and yield stress of 76 MPa [21].

The experimental study [34] on the quasi-static uniaxial crushing behavior of re-entrant hexagon honeycomb is used to validate the numerical model. **Fig**. 6 shows the comparison between the experimental and numerical results in terms of deformation modes and force-displacement curve. It is found that the model can well predict the deformation mode. Meanwhile, the numerical model yields a good agreement with the experimental results in the elastic and plateau stages, only with a slight delay of the densified stage. In general, the numerical model can predict crushing behaviors with good accuracy.

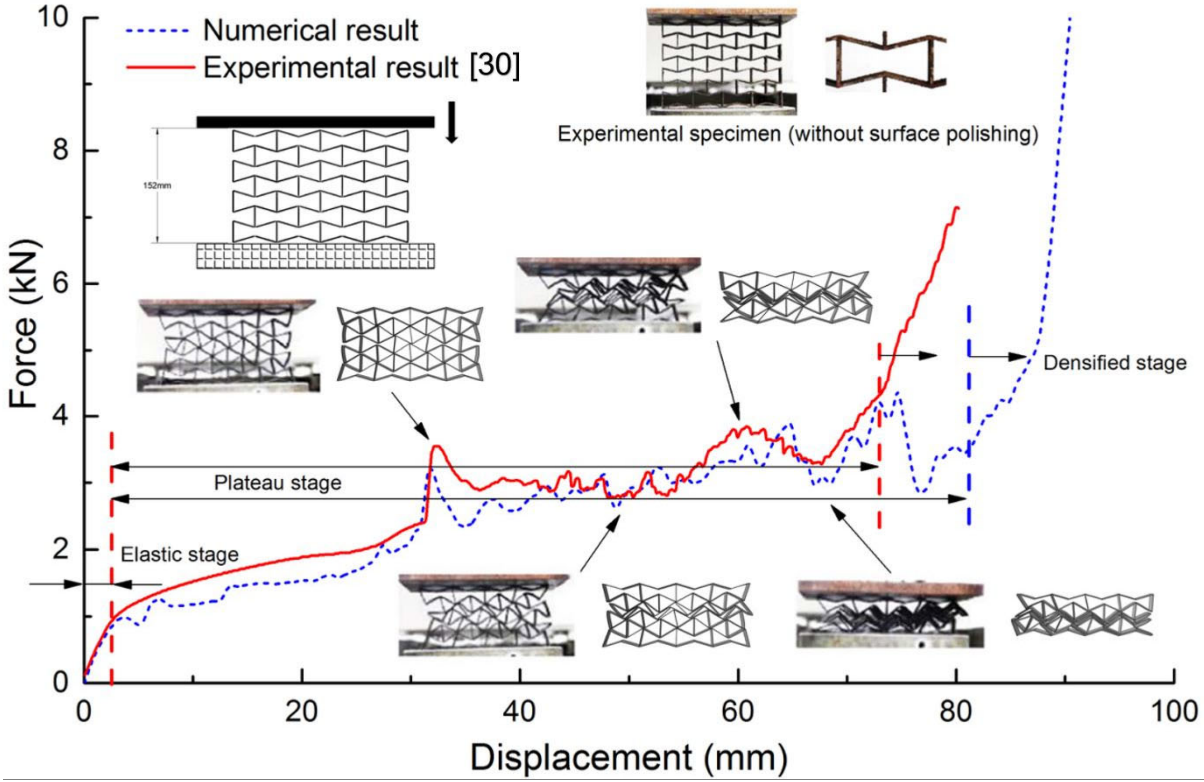

Fig. 6. Comparison between the results from experiment [34] and numerical study in terms of deformation modes and force-displacement curves.

4 Numerical results and discussions

As mentioned above, the topology of hexagonal cell affects the crushing behavior of honeycomb matrix. The unit cell dimensions L_x and L_y are kept the same for different cell topologies. The unit cell topologies with IPR from -3.3 to 3.3 are presented in **Fig**. 7 (a). It should be noted that given the cell wall thickness of 0.2 mm, the relative density of different honeycombs varies with IPR, as show in **Fig**. 7 (b). The influence of relative density on the crushing behavior is discussed in the following section.

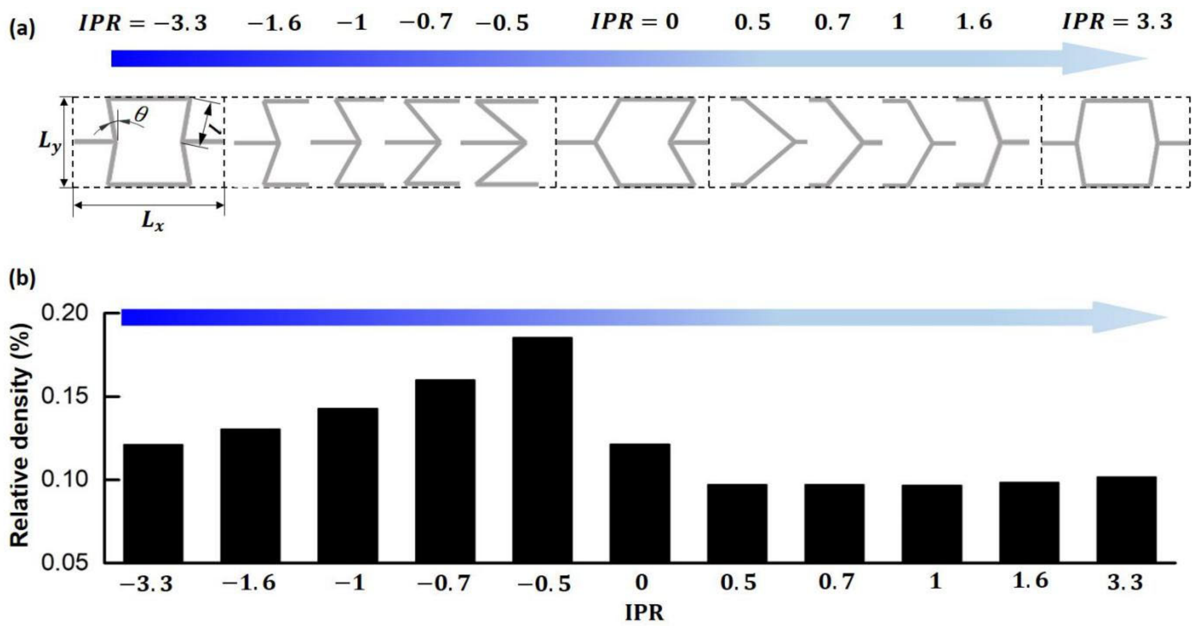

Fig. 7. (a) Schematic diagram of unit cells with different IPR values; (b) Relative density of unit cells with different IPR values.

4.1 Classification of deformation modes

Fig. 8 shows the map of typical deformation modes of the honeycombs with different IPR. The deformation modes are categorized into three types in green, grey and blue, named as mode 1, 2 and 3, respectively. **Fig**. 8 (a) shows the major difference between three modes. When the crushing speed is 5 m/s, the cell collapse bands initiate at both the proximal and distal ends, the deformation pattern with cross-shape is classified as mode Ⅰ. With the crushing speed increased to 15m/s, the cell collapse bands initiate at the proximal end only and such pattern is classified as mode Ⅱ. When the crushing speed reaches 70m/s, the cell collapse in a progressive manner from the proximal end (like an 'I' shape), the pattern is categorized into mode Ⅲ. The cross-shape collapse band in mode Ⅰ and Ⅱ is due to the lateral constraint effect of the honeycomb cell from center to the sides [35]. With zero IPR, the honeycomb experiences neither contracting nor expanding transversely and the lateral constraint effect is too weak to affect the deformation pattern, hence the cross-shape band is replaced by the progressive collapse band. It should be noted that honeycomb with zero IPR experiences no mode Ⅱ. **Fig**. 8 (b) shows the influence of IPR on the deformation modes of honeycombs and three columns represent mode Ⅰ, Ⅱ and Ⅲ, respectively. In mode Ⅰ, the collapsed bands gradually focus to the proximal end with the IPR increase in magnitude, as indicated in orange arrow in **Fig**. 8 (b). It implies that the honeycombs with the higher absolute value of IPR have higher wave impedance and the stress wave transmitted to the distal end is not intense enough to collapse more cells. The mode Ⅱ shows the opposite trend and the honeycombs with lower absolute value of IPR have higher wave impedance. In mode Ⅲ, the deformation modes are dominated by the stress wave propagation which are almost the same for different IPR values.

To identify the deformation mode regime, two sets of critical crushing speed are determined, termed as wave trapping and steady shock speed [35], respectively. Wave trapping speed V_W is the crushing speed at which the mode Ⅰ transfers to the mode Ⅱ, and the major difference is that the cell collapse bands initiate at the proximal end, instead of both ends. V_W is given as follows [35, 36]:

$$V_W = \int_0^{\varepsilon_{cr}} \sqrt{\frac{d\sigma_0}{d\varepsilon}\frac{1}{\rho^*}}\, d\varepsilon \tag{27}$$

where ε_{cr} is the strain of the first peak in the quasi-static stress-strain curve and ρ^* is the relative density of honeycomb. The steady shock speed V_S is given when the mode Ⅲ turns up with the cells collapsed in a 'shock' like manner ('I' shape collapsed band) [36]:

$$V_S = \sqrt{2\sigma_0\varepsilon_d/\rho^*} \tag{28}$$

where ε_d is the densified strain and its analytical model is given in the next section, . With Eq. (27) and (28), the general trend of fitting results in terms of critical crushing speed with respect to different IPR values are presented in **Fig**. 9. A classification map of deformation modes with respect to IPR values and crushing speed is given. It is found that the honeycombs with negative IPR generally have lower critical speed as compared to that with positive IPR of the same magnitude. Besides, honeycombs with higher absolute value of IPR associate with higher critical speed. Eq. (27) and (28) reveal that lower relative density (ρ^*) or higher static plateau stress (σ_0) can lead to the increase of critical speed. For honeycombs with the higher absolute value of IPR, lower relative density and higher static plateau stress can be achieved simultaneously. For example, the IPR -3.3 results in a lower relative density as compared to the IPR -0.5, as shown in **Fig**. 7 (b), it also has a higher static plateau stress as can be inferred from coefficient A in **Fig**. 5. The critical speed for the structure with IPR -3.3 is therefore higher than that with IPR -0.5. As reported in [36], the critical speed for deformation modes changing is determined by the shock wave trapping capability of honeycomb, which mainly depends on the micro-inertia effect of cells. The micro-inertia effect is determined by the relative density. The higher relative density yields more significant micro-inertia effect and a lower critical speed. This is the reason that the honeycomb with negative IPR has lower critical speed as compared to the honeycomb with positive IPR as shown in **Fig**. 9.

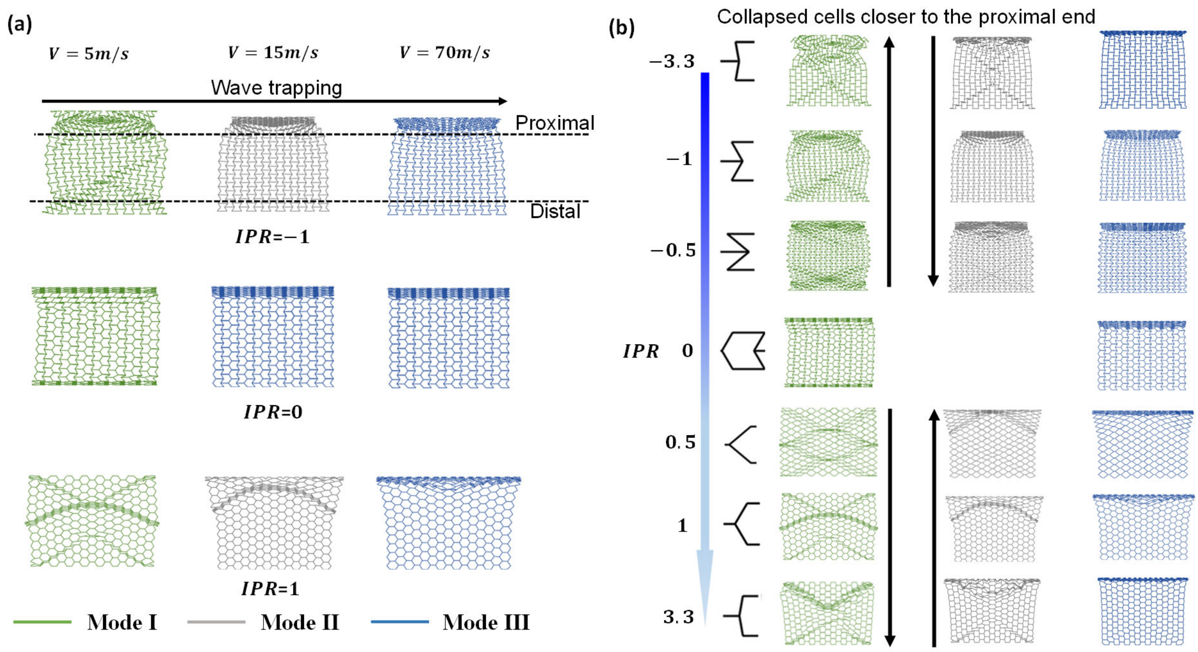

Fig. 8. (a) Deformation mode Ⅰ, Ⅱ and Ⅲ; (b) Influence of IPR on the deformation modes (green area: mode Ⅰ; grey: mode Ⅱ; blue: mode Ⅲ).

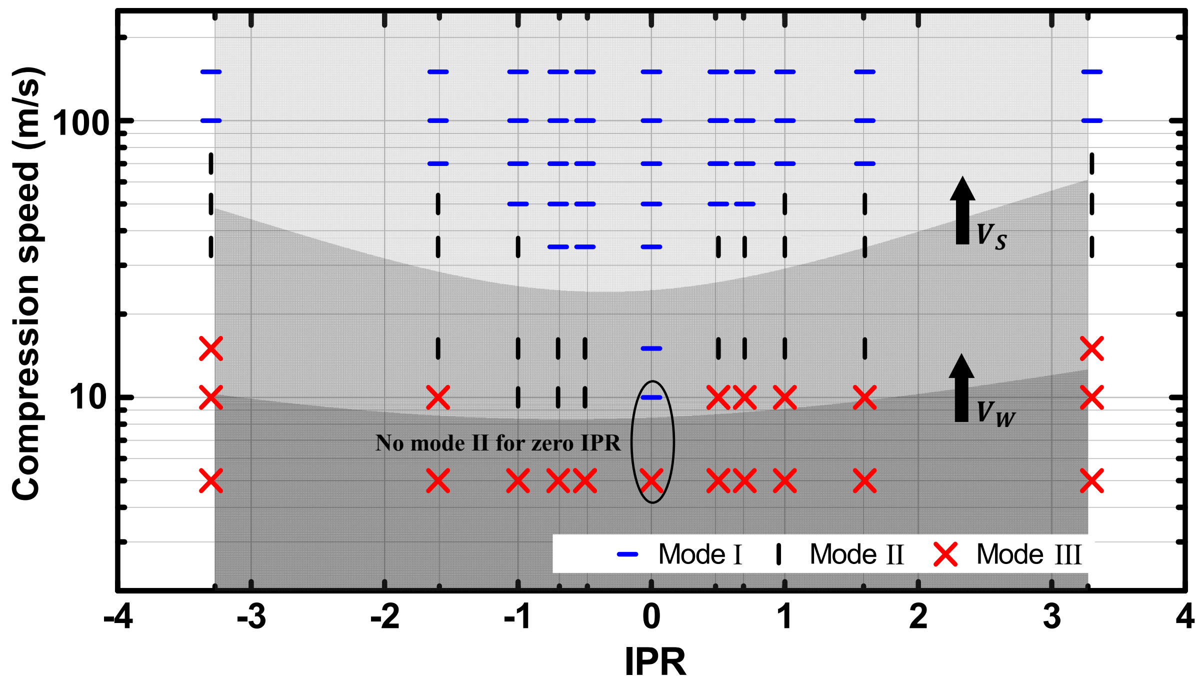

Fig. 9. Deformation-mode map with respect to IPR and crushing speed; critical speed of Vs, Vw (a lower critical speed represents a stronger micro-inertia effect).

4.2 Crushing behaviors

4.2.1 Plateau stress

Fig. 10 gives the typical engineering stress-strain curves with respect to different IPR values, in which engineering stress is defined as the ratio of contact force of proximal end to the original sectional scale of the honeycomb. From the previous studies [9, 21, 32], the crushing behavior in the plateau stage is the most concerned. The dynamic plateau stress is calculated as the average stress in the plateau stage. As shown in **Fig**. 10 (a) and (b), the plateau stress increases dramatically with the rising crushing speed. Higher crushing speed also induces more dramatic fluctuations of stress-strain curves. Densified strain is determined by the rapid rise point in the stress-strain curves and the densified strain increases with the rising crushing speed.

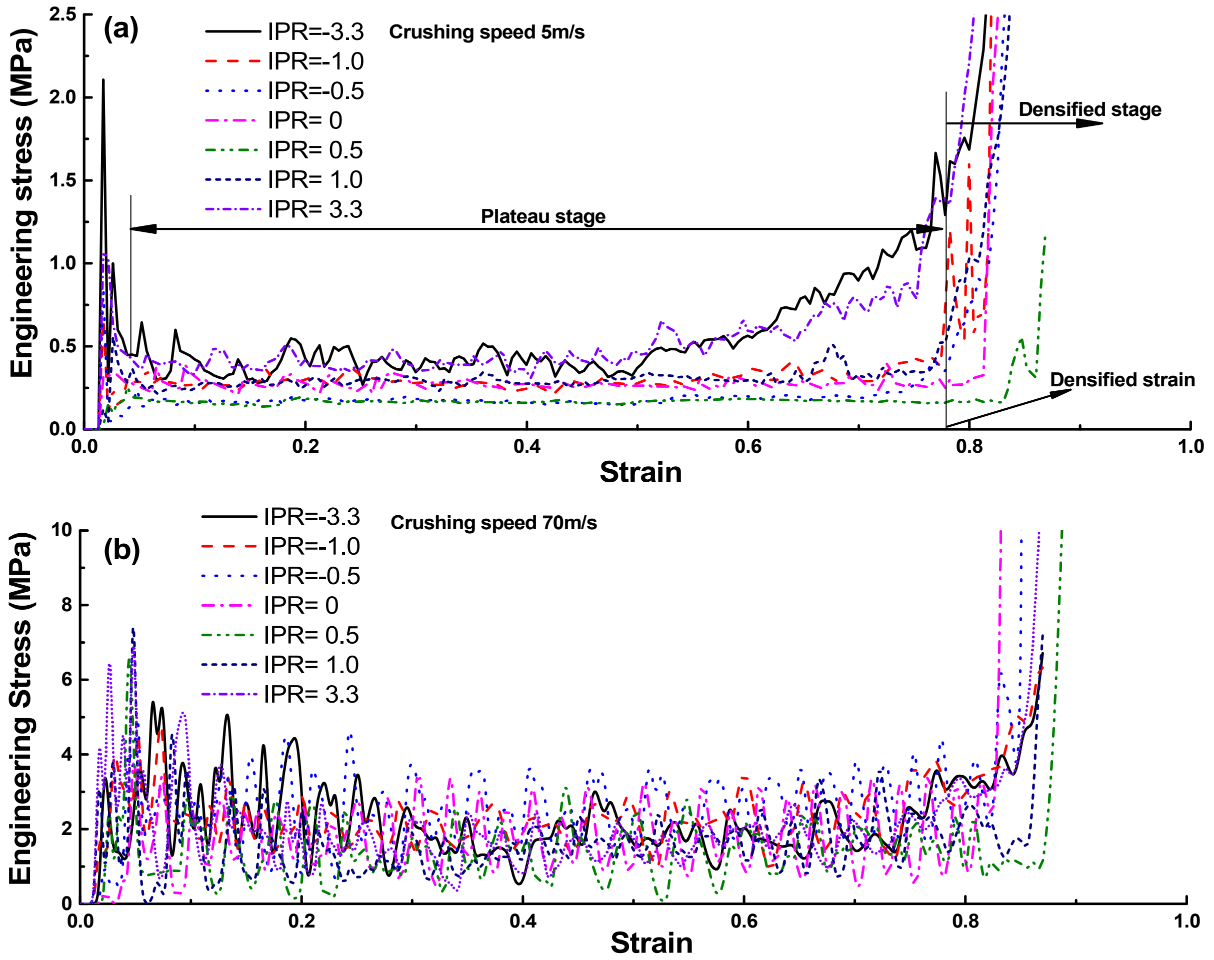

Fig. 10. Engineering stress-strain curve with respect to different IPR values: (a) 5m/s; (b) 70m/s.

Fig. 11 (a) gives the relationship of dynamic plateau stress σ_d and the IPR under various crushing speed. Generally, the dynamic plateau stress is significantly increased with the rising crushing speed, which is due to the strain rate enhancement induced by the micro-inertia effect. The influence of IPR on the dynamic plateau stress can be presented as below. When IPR $<$ -0.5, the dynamic plateau stress increases with the rising absolute value of IPR when the crushing speed changes from 5 m/s to 50 m/s, it decreases with the rising absolute value of IPR when the crushing speed changes from 70 m/s to 150 m/s. When $-0.5 \leq \text{IPR} \leq 0.5$, the dynamic plateau stress decreases with the rising IPR value, but when the crushing speed is below 35 m/s, the dynamic plateau stress jumps at the zero IPR. When IPR > 0.5, the dynamic plateau stress increases with the rising absolute value of IPR when the crushing speed changes from 5m/s to 35m/s. However, when the crushing speed is over 35m/s, the influence of IPR on the dynamic plateau stress is less significant. In addition, within the entire speed range (5 m/s -150 m/s), the dynamic plateau stress of structure with negative IPR is in general higher than that of positive IPR of the same magnitude due to the micro-inertia effect caused by higher relative density.

To better compare with the numerical results, coefficients A and B from the analytical model are presented in **Fig**. 11 (b). By comparing **Fig**. 11 (a) and (b), the relationship between coefficients and the dynamic plateau stress is very clear. With the crushing speed changing from 5 m/s to 15 m/s, the dynamic plateau stress in general follows the trend of static coefficient A. However, due to the sectional change induced by IPR effect is not considered in the analytical model, the relatively higher σ_d of negative IPR is not predicted by the static coefficient A. For example, the coefficient A is equal for honeycombs with IPR $= \pm 0.5$, but the plateau stress of IPR -0.5 is obviously larger than that of IPR 0.5 when crushing speed is 5 m/s. The reason for the jump of σ_d at zero IPR is that the zero IPR actually represents a series of topologies, but only one topology is studied herein which has the same θ and l as that of IPR $= \pm 1$. Hence, the coefficient A of zero IPR is similar to that of ± 1 and so does the dynamic plateau stress. Under relatively high crushing speed (e.g. 150 m/s), the trend of plateau stress is dominated by the dynamic coefficient B. It is well known that the stress enhancement under higher crushing speed is attributed to the micro-inertia effect of structures [21, 35, 36], and the micro-inertia effect is significantly affected by the relative density. The curve of relative density in **Fig**. 11 (b) indicates its influence on the coefficient B. However, the dynamic coefficient B is not only affected by the relative density but also the IPR effect, as the deviation between coefficient B and relative density is enlarged with the rising absolute value of IPR. As given in Eq. (15), the plateau stress is increased by shorter time interval $(t_1 - t_0)$ which can be calculated as $(H_0 - H_1)/V$. As shown in **Fig**. 11 (c), H_1 increases with the rising absolute value of IPR which results in a shorter time interval, the plateau stress (i.e. coefficient B) therefore improves more significantly. The deviation of the curves between coefficient B and relative density is enlarged.

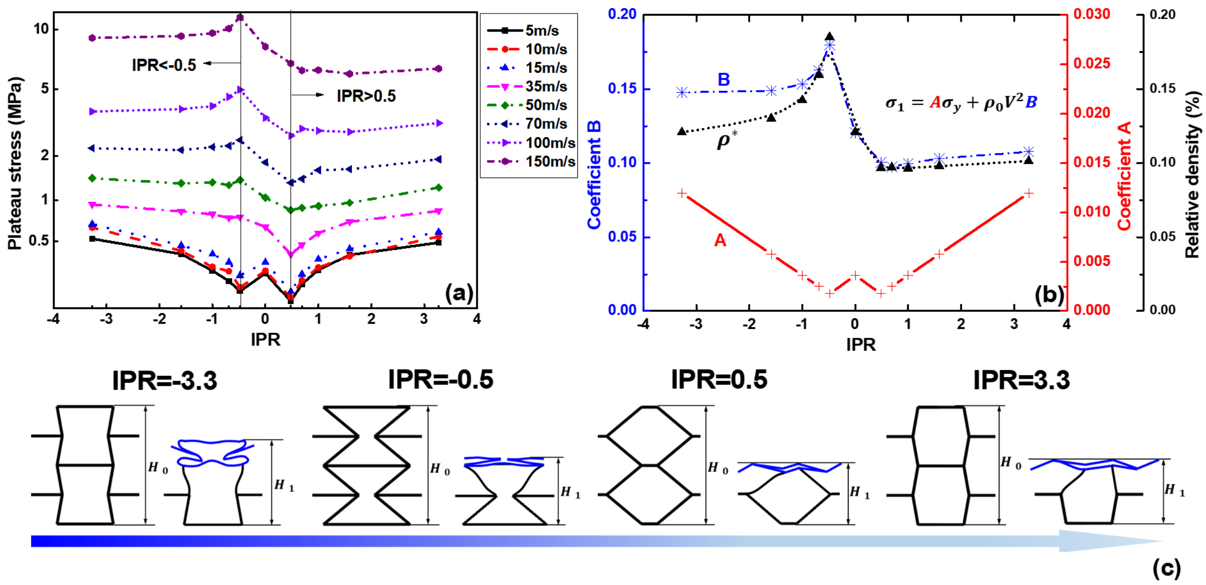

Fig. 11 (a) Variation of dynamic plateau stress with respect to IPR values and crushing speed; (b) Relative density and coefficients A (static) and B (dynamic) in Eq. (25) of honeycombs with different IPR values; (c) Representative deformation elements (RDEs) of honeycombs with IPR of ± 3.3 and ± 0.5.

To verify the accuracy of analytical model, the error δ of the dynamic plateau stress obtained from numerical simulation and analytical calculation, defined as $\Delta = 100\% \times (\sigma_1 - \sigma_d)/\sigma_d$, is used to verify the accuracy of analytical model. Since the sectional change induced by IPR effect is not considered in the RDEs, the analytical model underestimates the dynamic plateau stress of structure with negative IPR and overestimates that with positive IPR. The case with zero IPR yields good accuracy. By comparing the numerical results, the RDEs can be modified to further improve the accuracy of analytical model. From **Fig**. 4 (b), the height of RDE at $T = T_1$ is defined as $H_1 = 2l\cos\theta + \alpha t$ (Eq. (20)), where α is set as 4 for both the re-entrant and semi-re-entrant honeycombs, and 2.67 for the convex honeycomb in the original analytical model. However, as shown in **Fig**. 12 (a), it is reasonable to set $\alpha = 4$ for the case with IPR -0.5, but the height of collapsed cell increases for IPR -3.3 and α should also increase accordingly. For the positive IPR, α is derived from [23]: $\alpha = 1/\cos\omega$, where angle ω is a variant with different IPR values and its value can be derived by equating L_1 to the projection of the boundary ripples within the RDE in the lateral direction [23]. The corresponding value of the modified α is presented in **Fig**. 12 (b) and the error δ of dynamic plateau stress between the numerical results and analytical results using modified analytical model. It should be noted that only the results of mode Ⅲ are presented here. For the other two modes, the accuracy is relatively low because of the localized deformation assumption (as shown in **Fig**. 8 (a)) in the analytical model. It is found that the accuracy is improved with the rising crushing speed and it is reduced with the rising absolute value of IPR. In general, the modified analytical model can yield an acceptable accuracy (less than 10% relative error) to predict the dynamic plateau stress of honeycombs with the deformation mode Ⅲ.

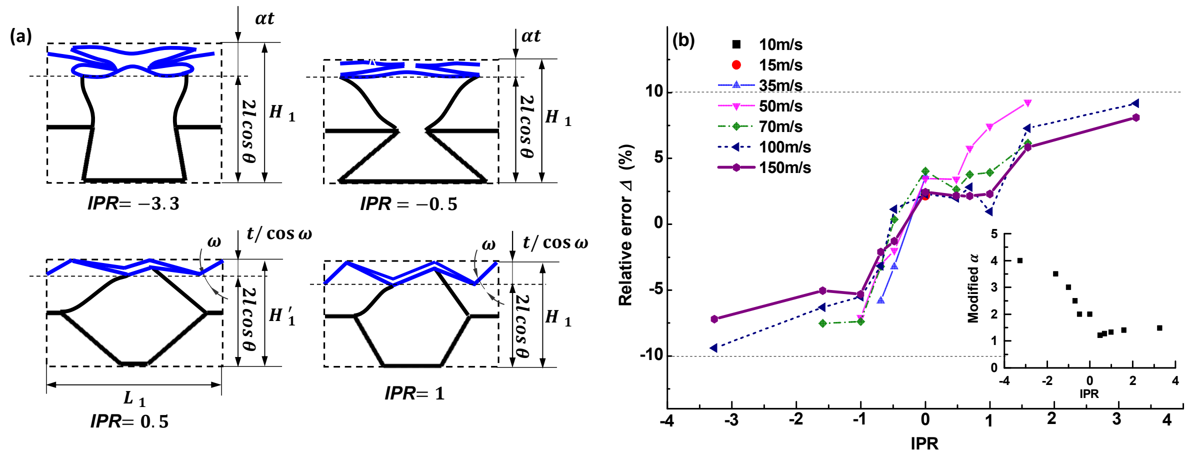

Fig. 12. (a) Schematic diagram of RDEs for modified analytical model (refer to **Fig**. 2 (a) for the geometry); (b) Relative error δ between the dynamic plateau stress of modified analytical model and numerical model (only the results for mode Ⅲ are shown).

4.2.2 Densification

Fig. 13 gives the densified strain which is defined by the rapid rise point in the stress-strain curves as shown in **Fig**. 10. The stress enhancement induced by the rising crushing speed results in the higher densified strain. Meanwhile, when the crushing speed further increase, the improvement of densified strain is less significant, since the deformed area tends to full densification. It should be noted that the crushing speed has less influence on the densified strain of zero IPR, attributed to its stable deformation mode evolution. **Fig**. 13 also shows that the higher IPR absolute value results in lower densified strain. This can be explained by the increased height of the compressed RDEs of honeycombs with the rising absolute value of IPR, as shown in **Fig**. 12 (a), which obviously results in a lower densified strain. In addition, because of the shrink behavior of the cells, the crushed honeycombs with negative IPR in general have larger residual height and lower densified strain , which was also reported in ref. [1].

According to Eq. (9), the dynamic plateau stress σ_d can be given as $\sigma_0 + \frac{\rho^*}{\varepsilon_d}V^2$ [32]. In the section 2.2, σ_d is determined by Eq. (24). By matching the term $\frac{\rho^*}{\varepsilon_d}V^2$ in Eq. (9) with the term related to V^2 of Eq. (24), and substituting the analytical expression of the relative density ρ^*, the analytical expression of the densified strain ε_d is given as below:

$$\varepsilon_d = \frac{(4l + 3h)(2l\cos\theta - \alpha t)}{4l\cos\theta\,(2l + h)} \tag{30}$$

The predicated ε_d by using Eq. (30) is given as the red solid line in **Fig**. 13. As compared with the numerical results, the analytical expression of ε_d is only related to the IPR values but not associated with the crushing speed. In general, the densified strain of honeycomb structure is mainly determined by its porosity (or relative density) [9]. However, different crushing speeds lead to various deformation modes, the analytical model gives a good prediction on the densified strain for mode Ⅲ, as shown in **Fig**. 9. The densified strain is slightly overestimated for mode Ⅰ and Ⅱ by using the analytical model due to the different deformation mode.

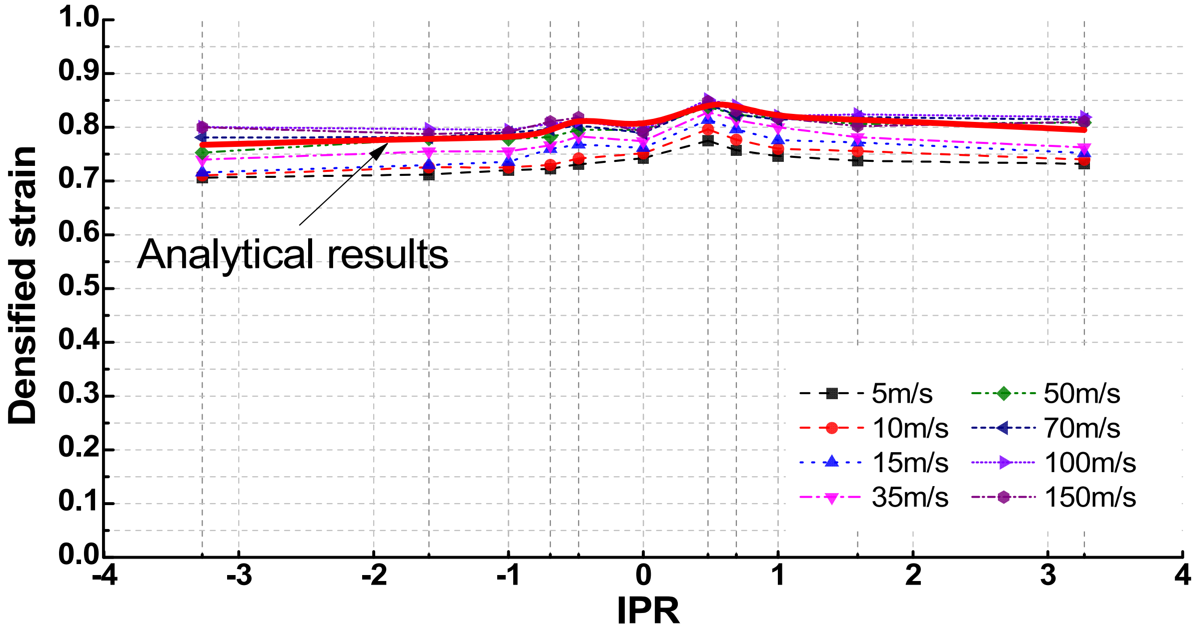

Fig. 13. Densified strain with respect to various IPR values and crushing speed. The red solid line represents the densified strain derived from analytical expression with respect to different IPR values.

4.2.3 Energy absorption

Energy absorption is defined as the enclosed area below the stress-strain curves as shown in **Fig**. 10. Hence, it is determined by both plateau stress and densified strain. Due to different relative density of honeycombs with various IPR, the specific energy absorption (SEA) is used to analyze the influence of IPR on the energy absorption capacity. **Fig**. 14 gives the SEA from numerical results with respect to IPR and crushing speed.

The rising crushing speed improves the SEA constantly due to the stress enhancement that is induced by inertia effect (as shown in **Fig**. 11 (a)). When the crushing speed changes from 5 m/s to 70 m/s, the SEA of honeycombs with different IPR values (except for the zero IPR) increases with the rising absolute value of IPR. However, the SEA decreases with the rising absolute value of IPR when the crushing speed is over 70 m/s. For example, the honeycomb with IPR -0.5 has the lowest SEA when crushing speed is 5 m/s, while it has the largest SEA when the crushing speed is 150 m/s. In addition, when the crushing speed changes from 5 m/s to 35 m/s, it is found that the SEA of structure with positive IPR is higher than that with negative IPR of the same magnitude (e.g. IPR $= \pm 1$). Although the plateau stress of structure with negative IPR is higher than that of positive IPR, the honeycomb with positive IPR has lower relative density and higher densified strain, as shown in **Fig**. 7 (b) and **Fig**. 13. Meanwhile, the variation of the plateau stress between honeycombs with different IPR is relatively small in this speed range, e.g. the variation between the plateau stress of IPR $= \pm 1$ is less than 0.05 MPa, as shown in **Fig**. 11 (a). When the crushing speed is over 35 m/s, the negative IPR yields higher SEA than the positive IPR of the same magnitude due to much higher plateau stress of negative IPR, as shown in **Fig**. 11 (a).

According to the previous work [22], a normalized plastic energy absorption $\overline{U}$ is used to analyze crushing speed effect on the energy absorption capacity. It normalizes the plastic energy absorption U by the ideal static plastic energy absorption. The ideal static plastic energy absorption is calculated as the energy dissipated by a completely crushed honeycomb under a quasi-static crushing speed which can be calculated as $\sigma_0 SL$, where σ_0 refers to the static collapse stress, S is the sectional area and L is the total length of honeycomb along the crush direction. The normalized plastic energy absorption $\overline{U}$ with respect to the crushing speed and IPR is plotted in **Fig**. 15. A higher value of $\overline{U}$ means that crushing speed effect has more significant improvement on the energy absorption of honeycomb. It is found that the honeycombs with negative IPR has more sensitive crushing speed dependency than that with the positive IPR of the same magnitude (e.g. IPR $= \pm 1$). It explains why the honeycomb with negative IPR gradually yields higher SEA than that with positive IPR when the crushing speed increases (as shown in **Fig**. 14). In addition, $\overline{U}$ decreases with the rising absolute value of IPR. The improvement on the energy absorption that induced by crushing speed is therefore more significant for the honeycomb with lower absolute value of IPR and the honeycomb with lower absolute value of IPR yields higher SEA when the crushing speed increases (as shown in **Fig**. 14).

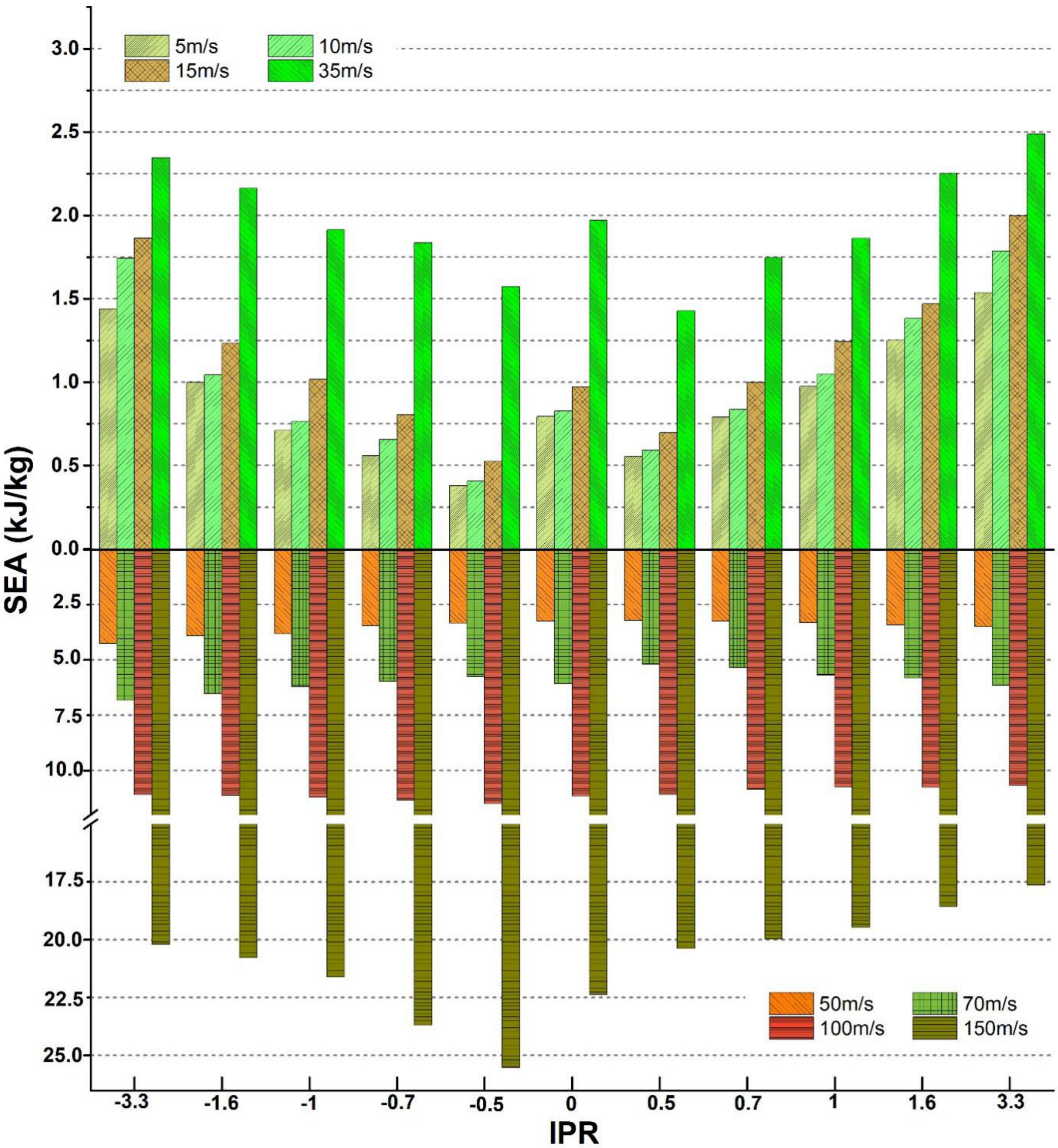

433

434 **Fig**. 14. Specific energy absorption (SEA) of honeycombs with respect to different crushing

435 speed and IPR values.

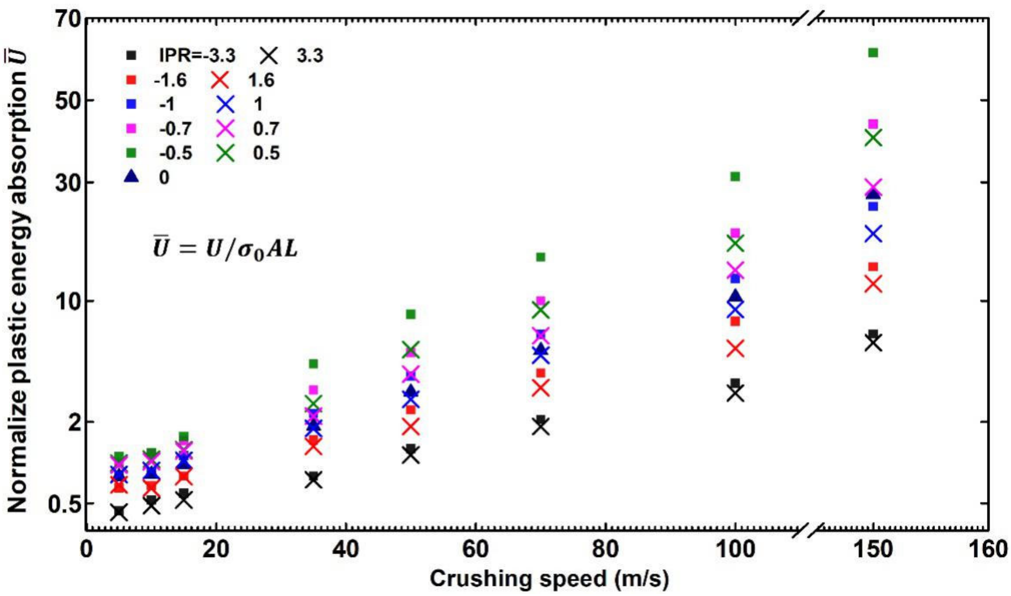

Fig. 15. Normalized energy absorption ($\overline{U}$) of honeycombs with respect to different crushing speed and IPR values.

5 Conclusions

In this study, the in-plane crushing behaviours of hexagonal honeycomb with different initial Poisson's ratios (IPR) are investigated through analytical and numerical methods. In the analytical study, the relationships between dynamic plateau stress and different IPR are derived. In the numerical study, comparative studies on various hexagonal honeycombs are conducted. The main findings can be drawn as below.

a) Three typical deformation modes (type I, II and III) under various crushing speeds are classified for the honeycombs with different IPR values. It should be noted the mode III is the most stable progressive deformation mode and the influence of material defect on the deformation mode is minimal among the three deformation modes. Two sets of critical speed are identified for the deformation mode changes from I to II and II to III, respectively [35]. It is found that the critical speed increases with the higher absolute value of IPR. In addition, the honeycomb with negative IPR yields lower critical speed as compared to that with positive IPR. The lower critical speed indicates that the honeycomb is prone to experience deformation mode III and a better shock wave trapping capability can be obtained [36].

b) When the crushing speed changes from 5 m/s to 50 m/s, the plateau stress σ_d in general increases with the rising absolute value of IPR. However, when crushing speed is over 50 m/s, the plateau stress decreases with the rising absolute value of negative IPR, while the positive IPR has less significant influence on it. In addition, the plateau stress of honeycomb with negative IPR is higher than that with positive IPR of the same magnitude (e.g. ± 1), the disparity is enlarged with the rising crushing speed. As found in the analytical study, the influence of IPR on the plateau stress is mainly achieved by affecting the micro-inertia effect and the collapsed cell shape.

c) SEA (Specific Energy Absorption) increases with the rising absolute value of IPR when crushing speed changes from 5 m/s to 70 m/s. However, the trend of SEA with respect to IPR is opposite when the crushing speed is over 70 m/s. The honeycombs with positive IPR can provide higher SEA than that with negative IPR of the same magnitude when the crushing speed is relatively low (5 m/s to 15 m/s). With the increasing crushing speed (from 35 m/s to 150 m/s), honeycombs with negative IPR exhibit better energy absorption capacity. The normalized plastic energy absorption shows that the honeycombs with the rising absolute value of IPR exhibit higher crushing speed sensitivity and the negative IPR in general exhibits higher speed sensitivity as compared to the positive IPR.

d) The honeycomb with zero IPR has the same cell wall geometry but different topology as that of $\text{IPR} = \pm 1$. It has higher plateau stress than that with $\text{IPR} = 1$ and lower than that with $\text{IPR} = -1$ at various crushing speeds. In addition, the honeycomb with zero IPR yields better energy absorption capability as compared to the honeycombs with IPR ± 1 at the higher crushing speed (e.g. 100 m/s, 150 m/s).

Acknowledgements

This work was financially supported by The National Science Foundation of China (51875581, 51505502), Huxiang Young Talents Plan (2019RS2004), Training Program for Excellent Young Innovators of Changsha, China (kq1802004), China Scholarship Council. The authors would like to express their thanks. The second author acknowledges the support from Australian Research Council via Discovery Early Career Researcher Award (DE160101116).

References

[1] W. Liu, N. Wang, T. Luo, et al. In-plane dynamic crushing of re-entrant auxetic cellular structure. Materials & Design, 2016. **100**: p. 84-91.

[2] Z. Li, W. Chen. H. Hao. Dynamic crushing and energy absorption of foam filled multi-layer folded structures: experimental and numerical study. International Journal of Impact Engineering, 2019. **133**: p. 103341.

[3] W. Chen. H. Hao. Experimental and numerical study of composite lightweight structural insulated panel with expanded polystyrene core against windborne debris impacts. Materials & Design, 2014. **60**: p. 409-423.

[4] Z. Li, W. Chen. H. Hao. Functionally graded truncated square pyramid folded structures with foam filler under dynamic crushing. Composites Part B: Engineering, 2019: p. 107410.

[5] Z. Li, W. Chen. H. Hao. Numerical study of blast mitigation performance of folded structure with foam infill. in Structures. 2019. Elsevier.
[6] Z. Wang, Z. Li. W. Xiong. Numerical study on three-point bending behavior of honeycomb sandwich with ceramic tile. Composites Part B: Engineering, 2019. **167**: p. 63-70.
[7] P. Li, Y. Guo, M. Zhou, et al. Response of anisotropic polyurethane foam to compression at different loading angles and strain rates. 2019. **127**: p. 154-168.
[8] P. Li, Y. Guo. V.J.I.J.o.I.E. Shim. Micro and meso-scale modelling of the response of transversely isotropic foam to impact—a structural cell-assembly approach. 2019: p. 103404.
[9] L.J. Gibson. M.F. Ashby, Cellular solids: structure and properties. 1999: Cambridge university press.
[10] G. Lu. T. Yu, Energy absorption of structures and materials. 2003: Elsevier.
[11] Z. Wang. Recent advances in novel metallic honeycomb structure. Composites Part B: Engineering, 2019.
[12] Z. Wang, Z. Li, C. Shi, et al. Theoretical and numerical analysis of the folding mechanism of vertex-based hierarchical honeycomb structure. 2019: p. 1-11.
[13] Z. Wang, Z. Li, Z. Wei, et al. On the influence of structural defects for honeycomb structure. 2018. **142**: p. 183-192.
[14] Z. Wang, Z. Li. W. Xiong. Experimental investigation on bending behavior of honeycomb sandwich panel with ceramic tile face-sheet. Composites Part B: Engineering, 2019. **164**: p. 280-286.
[15] Z. Wang. J. Liu. Numerical and theoretical analysis of honeycomb structure filled with circular aluminum tubes subjected to axial compression. Composites Part B: Engineering, 2019. **165**: p. 626-635.
[16] P. Li, Y. Guo, V.J.I.J.o.S. Shim, et al. A constitutive model for transversely isotropic material with anisotropic hardening. 2018. **138**: p. 40-49.
[17] B. Hou, Y. Wang, T. Sun, et al. On the quasi-static and impact responses of aluminum honeycomb under combined shear-compression. 2019. **131**: p. 190-199.
[18] B. Hou, A. Ono, S. Abdennadher, et al. Impact behavior of honeycombs under combined shear-compression. Part I: Experiments. 2011. **48**(5): p. 687-697.
[19] A. Bezazi, F. Scarpa. C. Remillat. A novel centresymmetric honeycomb composite structure. Composite Structures, 2005. **71**(3-4): p. 356-364.
[20] L.J. Gibson, M.F. Ashby, G. Schajer, et al. The mechanics of two-dimensional cellular materials. Proceedings of the Royal Society of London. A. Mathematical and Physical Sciences, 1982. **382**(1782): p. 25-42.
[21] D. Ruan, G. Lu, B. Wang, et al. In-plane dynamic crushing of honeycombs—a finite element study. International Journal of Impact Engineering, 2003. **28**(2): p. 161-182.
[22] A. Ajdari, H. Nayeb-Hashemi. A. Vaziri. Dynamic crushing and energy absorption of regular, irregular and functionally graded cellular structures. International Journal of Solids and Structures, 2011. **48**(3-4): p. 506-516.
[23] L. Hu. T. Yu. Dynamic crushing strength of hexagonal honeycombs. International Journal of Impact Engineering, 2010. **37**(5): p. 467-474.
[24] J. Liu, W. Chen, H. Hao, et al. Numerical study of low-speed impact response of sandwich panel with tube filled honeycomb core. Composite Structures, 2019. **220**: p. 736-748.
[25] Z. Wang, X. Wang, C. Shi, et al. Mechanical behaviors of square metallic tube reinforced with rivets—Experiment and simulation. 2019. **163**: p. 105118.
[26] S.A. Galehdari. H. Khodarahmi. Design and analysis of a graded honeycomb shock absorber for a helicopter seat during a crash condition. International Journal of Crashworthiness, 2016. **21**(3): p. 231-241.
[27] J.N. Grima, L. Oliveri, D. Attard, et al. Hexagonal Honeycombs with Zero Poisson's Ratios

and Enhanced Stiffness. Advanced Engineering Materials, 2010. **12**(9): p. 855-862.
[28] L. Hu, F. You. T. Yu. Effect of cell-wall angle on the in-plane crushing behaviour of hexagonal honeycombs. Materials & Design, 2013. **46**: p. 511-523.
[29] G. Imbalzano, S. Linforth, T.D. Ngo, et al. Blast resistance of auxetic and honeycomb sandwich panels: Comparisons and parametric designs. Composite Structures, 2018. **183**: p. 242-261.
[30] T. Li, Y. Chen, X. Hu, et al. Exploiting negative Poisson's ratio to design 3D-printed composites with enhanced mechanical properties. Materials & Design, 2018. **142**: p. 247-258.
[31] Y. Liu. X.-C. Zhang. The influence of cell micro-topology on the in-plane dynamic crushing of honeycombs. International Journal of Impact Engineering, 2009. **36**(1): p. 98-109.
[32] S. Reid. C. Peng. Dynamic uniaxial crushing of wood. International Journal of Impact Engineering, 1997. **19**(5-6): p. 531-570.
[33] X. Hou, Z. Deng. K. Zhang. Dynamic Crushing Strength Analysis of Auxetic Honeycombs. Acta Mechanica Solida Sinica, 2016. **29**(5): p. 490-501.
[34] Z. Zhou, J. Zhou. H. Fan. Plastic analyses of thin-walled steel honeycombs with re-entrant deformation style. Materials Science and Engineering: A, 2017. **688**: p. 123-133.
[35] Z. Zou, S.R. Reid, P.J. Tan, et al. Dynamic crushing of honeycombs and features of shock fronts. International Journal of Impact Engineering, 2009. **36**(1): p. 165-176.
[36] A. Hönig. W. Stronge. In-plane dynamic crushing of honeycomb. Part I: crush band initiation and wave trapping. International journal of mechanical sciences, 2002. **44**(8): p. 1665-1696.